# Patterns and trends in Chlorophyll-a concentration and phytoplankton phenology in the biogeographical regions of Southwestern Atlantic

**Ana L. Delgado[1,2], Ismael Hernández-Carrasco[3], Vincent Combes[3,4], Joan Font-Muñoz[3], Paula D. Pratolongo[5,6] and Gotzon Basterretxea[3]**

[1] Instituto Argentino de Oceanografía (IADO-CONICET-UNS), Bahía Blanca, 8000, Argentina.

[2] Departamento de Geografía y Turismo, Universidad Nacional del Sur (UNS), Bahía Blanca, 8000, Argentina.

[3] Institut Mediterrani d'Estudis Avançats (IMEDEA-CSIC-UIB), Esporles, 07190, Spain.

[4] Departament de Física, Universitat de les Illes Balears, Palma de Mallorca, 07071, Illes Balears, Spain.

[5] Centro de Recursos Renovables de la Región Semiárida (CERZOS-CONICET-UNS), Bahía Blanca, 8000, Argentina.

[6] Departamento de Biología, Bioquímica y Farmacia, Universidad Nacional del Sur (UNS), Bahía Blanca, 8000, Argentina.

Corresponding author: Ana L. Delgado (aldelgado@iado-conicet.gob.ar)

**Key Points:**

- Chlorophyll-a concentration has increased in the las 24-years in most of the Southwestern Atlantic.
- Phytoplankton phenological changes have been observed, mainly on the autumn bloom.
- Phytoplankton abundance and phenology might be affected by the sea surface temperature increase and the the mixed layer depth shoaling.

## Abstract

The Southwestern Atlantic Ocean (SAO), is considered as one of the most productive areas of the world, with high abundance of ecologically and economical important fish species. Yet, the biological responses of this complex region to climate variability are still uncertain. Here, using 24 years of satellite derived Chl-a datasets, we classified the SAO into coherent regions based on homogeneous temporal variability of Chl-a concentration, as revealed by the SOM (Self-Organizing Maps) analysis. These coherent biogeographical regions were the basis of our regional trend analysis in phytoplankton biomass, regional phenological indices, and environmental forcing variations. A generalized positive trend in phytoplankton concentration is observed, especially in the highly productive areas of the northern shelf-break, where phytoplankton biomass is increasing at an outstanding rate up to $0.42 \pm 0.04$ mg $m^{-3}$ per decade associated with the sea surface temperature (SST) warming ($0.11 \pm 0.02$ °C $decade^{-1}$) and the mixed layer depth shoaling ($-3.36 \pm 0.13$ m $decade^{-1}$). In addition to the generalized increase in chlorophyll, the most sticking changes in phytoplankton dynamics observed in the SAO are related to the secondary bloom that occurs in most of the regions ($15 \pm 3$ and $24 \pm 6$ days $decade^{-1}$) which might be explained by the significant warming trend of SST, which would sustain the water stratification for a longer period, thus delaying the secondary bloom initialization. Consistent with previous studies, our results provided further evidences of the impact of climate change in these highly productive waters.



## Plain Language Summary

The Southwestern Atlantic Ocean (SAO), is one of the most biologically productive areas of the world, with high abundance of fish species. This important area might be affected by the environmental consequences of climate change. In this study we addressed the influence of the already observed changes in environmental conditions on the phytoplankton, which is the base of the marine food web, in the last 24 years. There is an increase in phytoplankton abundance as well as the timing and intensity of the autumn bloom in some specific areas of the SAO. We have found that these changes might be related to the increase of sea surface temperature and the shoaling of the mixed layer depth, which is the upper layer of the ocean, which is directly influenced by the atmospheric processes. Consistent with previous studies, our results provided further evidences of the impact of climate change in these highly productive waters.


## 1 Introduction

Phytoplankton is at the base of the marine food webs and plays a major role on the global $CO^2$ fluxes. Indeed, marine phytoplankton roughly produces 50 Gt of organic C $yr^{-1}$, corresponding to ~ 40 % of the annual global primary productivity contributing to the uptake of more than 23 % of the total anthropogenic $CO^2$ emissions into the atmosphere (Friedlingstein et al., 2019). Phytoplankton community species composition, initiation, duration and therefore intensity of blooms and the overall productivity of the oceans are predicted to change in response to variations in water temperature, nutrients supply, and acidification derived from the ongoing climate change (Doney et al., 2012). Phytoplankton growth is mostly controlled by light and nutrient availability and therefore, tightly linked to the dynamics of the ocean surface mixed layer (Longhurst, 2007). Atmospheric forcing and large-scale climate variability pattern, together with top-down controls (i.e. grazing), modulate phytoplankton phenological cycles (Zhai et al., 2013). Thus, the long-term variations in phytoplankton phenology may be used as indicators to

assess how variations in the marine environment propagate from primary producers to higher trophic levels. However, anticipating how these changes will occur in a future ocean remains challenging, as phytoplankton includes phylogenetically diverse organisms with disparate metabolic responses and evolutionary backgrounds (Dutkiewicz, et al., 2013; Anderson et al., 2021).

The Southwestern Atlantic Ocean is a vast sink for atmospheric and anthropogenic $CO^2$ via biological and solubility pump processes (Sigman et al., 2010), and is regarded as one of the most important regions for the global carbon cycle. This is largely due to the high biological productivity that results from its intense hydrodynamics and biogeochemical features (Field et al., 1998). The Patagonian shelf, which extends from the tip of South America (~55°S) to the Brazil/Malvinas Confluence (~38°S), occupies less than 2 % of the Southern Ocean surface. Yet it is one of the most biologically productive regions and largest carbon sink in the world, and one of its potentially most important sources for iron fertilization to the rest of the Southern Ocean (Fig.1, García et al., 2008; Lutz et al., 2010). This region is characterized by the presence of intense frontal systems driven by the combination of different physical processes (i.e. coastal upwelling, thermo-haline circulation, tidal forcing; Acha et al., 2004) which can lead to strong phytoplankton blooms, mainly dominated by diatoms, coccolithophores and dinoflagellates (e.g. Alvain et al., 2008; Guinder et al., 2018; Segura et al., 2021; Delgado et al., 2019). As a result of climate change, the region is showing clear evidence of environmental changes, largely associated with an increase in sea surface temperature (SST; Hobday and Pecl, 2014), changes in wind patterns (Leyba et al., 2019), the poleward migration of western boundary currents (Artana et al., 2019) and intensification and/or increase in the frequency and intensity of climate variability events (ENSO, Southern Annular Mode, droughts, heatwaves; e.g. Cai et al., 2020; Risaro et al., 2022).

The classification of marine areas into biogeographical regions sharing a similar dynamic has become essential to understand the responses of marine ecosystems in highly complex areas, such as the SAO, to environmental forces in present and future climate scenarios (Basterretxea et al., 2018). In addition, classification of the marine environment into biogeographic regions contributes to the understanding of ecosystem functions, very useful to define local (or specific) indicators of ecosystem state, supporting the establishment of resource management and conservation policies (Spalding et al., 2007). Satellite ocean-color data provides synoptic and long-term coverage, which is ideal for regionalization studies. The Self-Organizing Maps (SOMs), a neural network-based technique developed in the last decades, has proven very effective to cluster and identify patterns in large datasets (Kohonen, 1982; Vesanto and Alhoniemi, 2000). SOM classification method has been used for a variety of applications including the synthesis of spatial patterns of chlorophyll-a (Chl-a) and its variation and the classification of spectral signals for subsequent inference of phytoplankton groups (e.g. Saraceno et al., 2006; Ben Mustapha et al., 2014; Basterretxea et al., 2018; Yala et al., 2020). SOM can be applied to both space and time domains of the analysed variable, providing, a powerful analysis tool for diagnosing ocean processes (Liu et al., 2016, Hernández-Carrasco and Orfila, 2018).

The present work aims at characterizing the spatial patterns and long-term trends of Chl-a concentration and phytoplankton phenology in the Southwestern Atlantic Ocean, and their relation with on-going climate-induced environmental changes in the Southwestern Atlantic. Using 24 years of satellite derived Chl-a datasets, we first classified the SAO into coherent regions based on homogeneous temporal variability of Chl-a concentration, as revealed by the

SOM analysis. These coherent biogeographical regions were the basis of our regional trend analysis in phytoplankton biomass, regional phenological indices, and environmental forcing variations. The observed changes in phytoplankton biomass and phenology, as well as the related environmental changes, are key to understand regional functional and structural aspects of marine communities in the SAO, allowing to set a potential strategy to detect and monitor crucial regions.

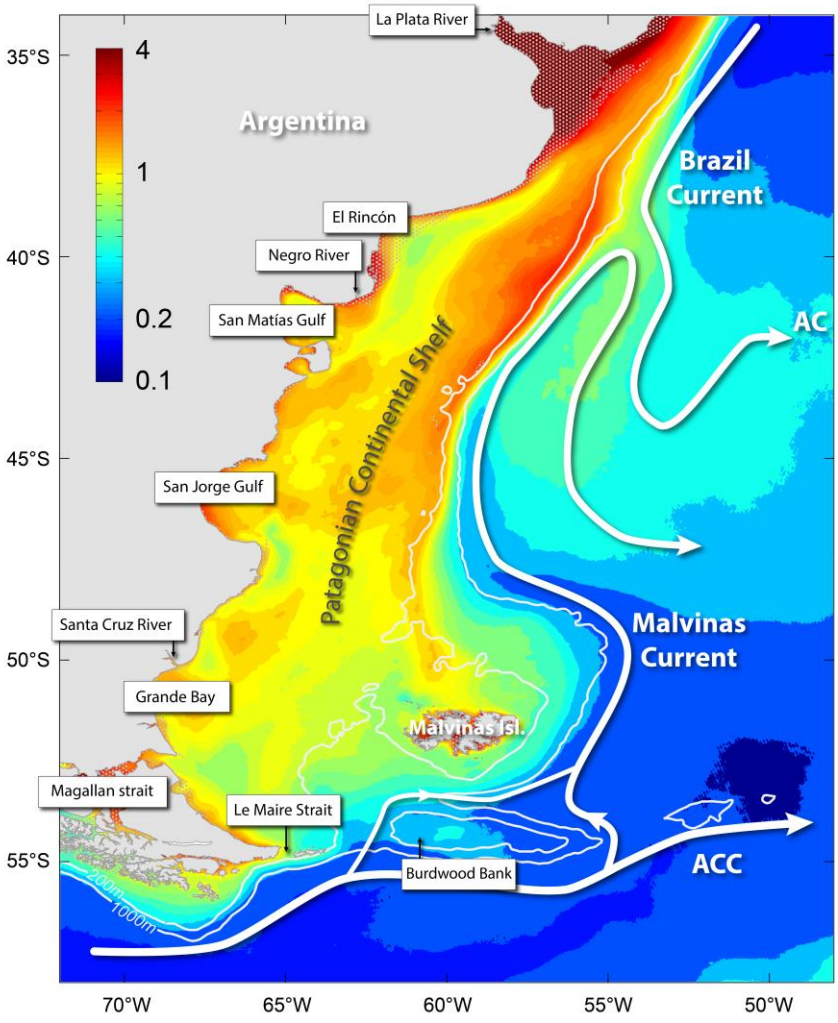


**Figure 1.** Mean Chlorophyll-a concentration (mg $m^{-3}$) in the Southwestern Atlantic Ocean (SAO) for the period (1998-2021) and, overlapped, main circulation patterns (thick arrows). Doted areas indicate biased chlorophyll-a values that were excluded from the analysis.

## 2 Materials and Methods

### 2.1 Data sources

Our analysis is based on the sea surface Chl-a (mg $m^{-3}$) merged product provided by the GlobColour project (distributed by ACRI ST, France: https://hermes.acri.fr/). A spatial subset of the study area (Fig.1) was extracted from a time series of the 8-day L3 Chl-a product at 4 km

resolution for the period 1998-2021 (24 years). This ocean color product is the result of merging SeaWiFS, MERIS, MODIS-Aqua and OLCI sensors and estimates the average Chl-a concentration over the first optical depth (Maritorena et al., 2010). Merging data from different satellite sensors is an effective method for increasing the study period of ocean color satellites to access climatic studies (Maritorena and Siegel, 2005). The Chl-a algorithms used to develop this product were validated in the Southwestern Atlantic Ocean with in situ data acquired between 2001 and 2019 obtaining accurate results (Delgado et al., 2021, $R^2$= 0.84; Dogliotti et al., 2009, $R^2$=0.89; Ferreira et al., 2013, $R^2$=0.75). Moreover, the GlobColour merged product presents a good accuracy with in-situ Chl-a data ($R^2$=0.81, Bias=0.03; Garnesson et al., 2022). Even though this product has not been climatology bias corrected, as OC CCI (Sathyendranath et al., 2019), both products present similar accuracy results (Yu et al., 2023), plus GlobColour flag strategy allows a higher spatial and temporal covering (Garnesson et al., 2019). Since global algorithms (based on blue-to-green ratios) do not perform well in the optically complex waters of the inner Argentinean Continental Shelf (Armstrong et al., 2004; Delgado et al., 2021; Williams et al., 2013), we masked the coastal waters located at depths < 25 m to avoid biased results.

Physical variables used for the environmental characterization were obtained from the Global Ocean Physics Reanalysis provided by CMEMS (GLORYS12v1). GLORYS provide monthly Sea Surface Temperature (SST), monthly Mixed Layer Depth (MLD) and Sea Surface Salinity (SSS), among other physical variables, at 1/12° spatial resolution. GLORYS12 is available in Copernicus Marine Environment Monitoring Service (CMEMS, https://data.marine.copernicus.eu) and is based on the current real-time global high-resolution forecasting CMEMS system PSY4V3 (Lellouche et al., 2018). The model outputs have proved to present accurate results for trend analysis (SST, bias < 0.01°C; SSS, bias < 0.2; Drévillon et al., 2022).

### 2.2 Biogeographical regionalization

Biogeographical regions within the study area were defined based on the analysis of satellite derived Chl-a using Self-Organizing Maps (SOM). SOM is a type of artificial neural network that is trained using an unsupervised learning algorithm. This technique is especially suited for feature extraction and pattern recognition in large datasets (Kohonen et al., 1982; 1990). SOM is a nonlinear mapping method that projects high-dimensional data onto a low dimensional space, preserving the topology of the original dataset. As a result, SOM can summarize the information contained in large time series of georeferenced variables, into a single map of a few patterns (Liu et al., 2016). When SOM is applied to the time domain of Chl-a satellite data, distinctive temporal patterns of Chl-a concentration can be inferred, allowing the identification of regions having a similar phytoplankton dynamics (Basterretxea et al., 2018).

We selected a network or map, of 3 x 3 neurons or units. Increasing the number of neurons, for instance using a neural network of size of 4 × 4 and 4 x 3, we obtain more detailed temporal patterns, and more regions of Chl-a variability emerge. However, these new patterns only split the boundaries of regions inferred from the 3x3 SOM, without providing relevant insight into regions with different biochemical or physical behaviour. Furthermore, as reported in Liu et al. (2006) and also seen in Basterretxea et al. (2018) and Hernández-Carrasco and Orfila (2018),

using larger number of neurons can result in fictitious patterns (with zero probability of occurrence), which are not representative of the analysed data set.

In our computations we use a sheet and hexagonal map lattice configuration, guaranteeing that the distance between the neuron and all its associated neighbours is the same. Each neuron has assigned a weighted vector of Chl-a values randomly generated during the initialization. In the training process the neural network is transformed through an iterative presentation of the satellite Chl-a data, previously normalized. In each iteration (or epoch), the neuron whose weight vector is more similar (in terms of Euclidean distance) to the input data vector, called Best-Matching Unit (BMU), is updated together with its topological neighbours towards the input sample following a neighbourhood function. Following Liu et al. (2006), we opted for a 'Ep' type neighbourhood function and a batch training algorithm, as this combination yields the best accurate patterns (i.e. lower quantitative and topological errors) and low computational cost. After repeating the training process iteratively (100 epochs in our case), until a stable convergence of the map is achieved, we obtain a neural network with the final time variability patterns of Chl-a concentration. The resulting patterns will exhibit some similarity because the SOM process assumes that a single sample of data (one input vector) contributes to the creation of more than one pattern, as the whole neighbourhood around the best matching pattern is also updated in each step of training. We have used the SOM v.2.0 MATLAB toolbox (Vesanto et al., 2000) distributed by the Helsinki University of Technology (http://www.cis.hut.fi/somtoolbox/) and adapted to long time series of satellite data.

### 2.3 Phytoplankton phenology

Phytoplankton phenology was analysed using the characteristic Chl-a time series obtained for each biogeographical region from the SOM analysis. The obtained SOM time series was processed with TIMESAT software, which was developed to explore time series of vegetation indices with a regular cyclicity and to retrieve the phenology metrics (Jönsson and Eklundh, 2004; Palmer et al., 2015). TIMESAT has been successfully applied to study phytoplankton phenology in diverse aquatic environments (Benzouaï et al., 2020; Palmer et al., 2015; Shi et al., 2019). The characteristic time-series was low-pass filtered with a Savitzky-Golay filter (window size 4) to reduce high frequency chlorophyll variations. The start-end season methodology used for our data, was the common definition of the start bloom event when Chl-a concentration rise above background median concentration plus a percentage oscillating between 5 to 20 % depending on the phytoplankton biomass of the region (Recault et al., 2012; Zoljoodi et al., 2022). Since in our case the Chl-a concentration is relatively high (0.1 - 14 mg m-3) and we wanted to avoid small peaks, we chose the 20 % above the median to identify the start and the end of the bloom season. Four essential indices proposed by Recault et al. (2012) were used to characterize phytoplankton phenology; the timing of the main bloom initiation ($b_i$), the peak intensity ($p_k$), the timing of main bloom period termination ($b_e$) and the bloom duration. The same indices were used when a secondary bloom was observed.

### 2.4 Trend analysis

Census X-13 seasonally adjusted methodology U.S. Census Bureau (2017) was used to remove seasonality from the characteristic Chl-a time series of each biogeographical region. The Census X-13 is an improved version of Census X-11, whose application to time-series analysis of

satellite ocean color data has been extensively documented (Delgado et al., 2015; Salgado-Hernanz et al., 2019; Vantrepotte and Mélin, 2009). The method is based on the iterative bandpass- filtering procedure that allows for the definition of a non-periodical seasonal term, in order to specifically assess the inter-annual variation in the time series seasonality (in terms of period and amplitude). The relative part of the variance of the components is estimated for each grid point, to identify the spatial patterns of the temporal variability in the series. This method aims at decomposing a time series X(t) (i.e. Chl-a, phenological metrics, environmental forcing parameters derived from each biogeographical region) into three additive components: S(t), the seasonal signal, T(t), the trend cycle, and I(t), the irregular o residual signal (Shiskin, 1978; Vantrepotte and Mélin, 2009).

Three successive steps are applied to decompose the time series. First, an estimation of the trend-cycle component was obtained from the annual-centred running average, and a seasonal running mean was subsequently applied to the trend series to acquire the seasonal component. Then, the series were normalized by subtracting the annual-centred running mean and the revised estimates are obtained, applying a Henderson filter of weight to the seasonal adjusted series. Finally, estimates of the trend and irregular component were calculated, repeating the application of the seasonal running mean and the Henderson filter on the revised trend adjusted series (Vantrepotte and Mélin, 2009).

Trends on the T(t) component of Chl-a, SST, MLD, SSS and on the yearly phenological estimates ($b_i$, $p_k$, $b_e$ and $b_d$) were calculated for each biogeographical region. In order to detect trends and to check its consistency we employ the Sens's method and the non-parametric seasonal Kendall statistics technique, allowing to accept or reject the presence of significant monotonic long-term change in the time series obtained from the Census X-13 method. The test relies on the computation of a suite of Mann-Kendall statistics applied monthly which finally is combined to detect the presence of long-term monotonic changes in the original time series (Vantrepotte and Mélin, 2011). The amplitude of the changes was assessed using the non-parametric Sen's slope estimator expressed in mg $m^{-3}$ $decade^{-1}$ (Chl-a, $p_k$), days $decade^{-1}$ ($b_i$, $b_e$ and $b_d$), m $decade^{-1}$ (MLD) and Celsius degrees $decade^{-1}$ (SST) (Gilbert, 1987; Ibañez and Conversi, 2002).

## 3 Results

### 3.1 Biogeographical regionalization

The 9 biogeographical regions and their corresponding characteristic temporal patterns and climatology obtained from the SOM analysis are shown in Fig. 2. The patterns are topologically ordered according to the mean value and variance. For instance, patterns with large variability and higher mean values of Chl-a concentration are located at the top-right corner of neural network, whereas those with low variability and low mean Chl-a concentrations, are located around the bottom-left corner.

The less productive regions (R1, R2, and R3) jointly comprise 66 % of the study area and mainly represent oceanic waters off the shelf. R3 is characterized by the lowest mean Chl-a concentration and variability of the whole study area ($0.41 \pm 0.18$ mg $m^{-3}$) and includes the southern section of the study area where the Antarctic Circumpolar Current flows through the

Drake Passage and the Burdwood Bank. R1 is the second largest region, extending over 22 % of the study area. Mean Chl-a concentration in this region is twofold that in R1 (0.83 ± 0.36 mg $m^{-3}$). Most of the coastal Patagonian tidal fronts, from the southern portion of San Matías Gulf until Grande Bay (southern margin of Argentina) lie within R1, as well as the northern retroflection of Malvinas Current (MC; Fig.1). R2 corresponds to the northern inner shelf waters of the study area (El Rincón and Norpatagonian Gulfs) and to the oceanic waters located outside the shelf break northern 44° S (0.74 ± 0.29 mg $m^{-3}$), where the retroflection of Brazilian Current is located (R1).

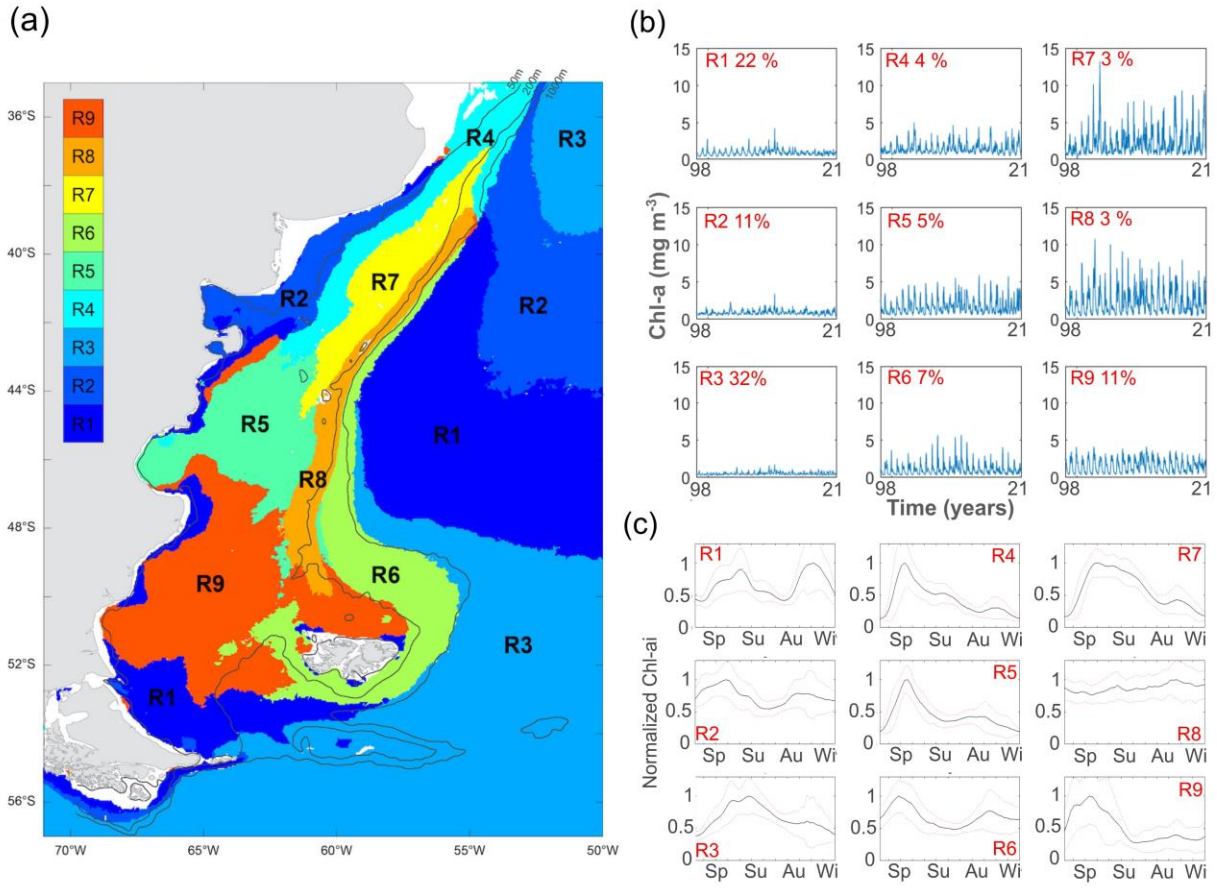


**Figure 2.** (a) Biogeographical classification Chl-a depicted from the 3 x 3 Self-Organizing Map (SOM) classification. (b) Characteristic Chl-a temporal patterns obtained from SOM computation. Inset number in red indicate the percentage of pixels clustered in each neuron. (c) Normalized climatology of the Chl-a temporal patterns. The black line stands for the mean values and the red-dashed line for the standard deviation. Sp=Spring, Su=Summer, Au=Autumn, Wi=Winter.

R4 and R5 represent transition regions between the open ocean waters and the highly productive regions over the southern shelf and shelf break. R4 is geographically located in the mid-shelf waters of Northern PCS. AS compared with the previous described regions, the mean value of

Chl-a concentration and variability are higher (1.37 ± 0.7 mg $m^{-3}$). Region R5 highly productive region (1.52 ± 0.97 mg $m^{-3}$) encompasses the San Jorge Gulf and La Isla Escondida area.

Regions characterized by patterns shown in the upper right corner of the neural network (R7, R8 and R6, Fig.2b-c) represent the main hot spots of primary production in the Southwestern Atlantic Ocean, with chlorophyll-a concentrations exceeding in some cases 10 mg $m^{-3}$. The SOM analysis identifies three distinct subzones in this frontal area. Region 7 represents the north-western section of the SBF, between 37 and 44 °S and located in the mid-shelf/outer-shelf, within the Argentinean Continental waters (2.08 ± 1.7 mg $m^{-3}$). R8 spans along the shelf-break, between ~38º and 49° S, with outstanding mean Chl-a concentrations (2.13 ± 1.65 mg $m^{-3}$). Finally, R6 extends between the 200 and 1000 m isobath, from 40 °S to the north-western border of the Malvinas Islands. This region exhibits mean values of Chl-a comparable to R1, R2 and R3 but higher variability (0.92 ± 0.75 mg $m^{-3}$).

Finally, R9 presents some similarities to R6, according to topological ordering of SOM. This region encompasses the Patagonian cold estuarine zone, off the coast of southern Patagonia, characterized by relatively high mean values and variability of Chl-a concentration (1.4 ± 0.9 mg $m^{-3}$). R9 extends from the outer region of the Peninsula Valdez front to the northern area of the Malvinas Islands, where it overlaps with the southern boundary of the SBF.

### 3.2 Phytoplankton phenology

Phytoplankton phenology indexes are displayed in Fig.3. All regions present a main seasonal bloom in austral spring (Sep – Dec). Additionally, some regions show a secondary peak in austral autumn (Mar– Jun; Fig.3). It is worth mention that bloom detection was based in threshold values, and for some regions there were calendar years in which blooms were not detected. This was more common for the secondary bloom, which occurred in 33-87 % of the years depending on the region (supplementary material, Table S1-S2).

Although R3 presents relatively low Chl-a values, two blooms were identified, one in spring-summer (16$^{th}$ Oct- 8$^{th}$ Feb) with mean bk of 0.7 mg $m^{-3}$, and a secondary bloom in autumn-winter ($b_k$ = 0.63 mg $m^{-3}$; 7$^{th}$ May – 5$^{th}$ Aug). Also, R2 is characterized by two blooms with similar intensity, one in spring ($b_k$ = 1.14 mg $m^{-3}$; 5$^{th}$ Sep – 28$^{th}$ Dec) and one in autumn ($b_k$ =0.94 mg m-3; 18$^{th}$ Apr – 30$^{th}$ Jun). Frontal zones in R1 present a semi-annual cycle, more productive in late spring-summer, with a bloom starting by the end of November (28$^{th}$) and spanning for 107 days with a peak intensity of 1.36 mg $m^{-3}$.

The seasonal pattern of Patagonian temperate fronts in R5 agrees with the canonical cycles of temperate seas, where the chlorophyll maxima occurs when the water column stabilizes in early spring (26$^{th}$ Sept – 5$^{th}$ Jan) and a secondary bloom that takes place during fall (27$^{th}$ Mar- 30$^{th}$ May). The mean bk in spring is one of the highest blooms among all inferred SOM regions, 3.79 mg $m^{-3}$. Similarly, maximum phytoplankton concentrations at R4 starts in early-spring ($b_i$ = 27$^{th}$ Aug) and spans for 91 days reaching a bk of 2.48 mg $m^{-3}$. During fall, the peak is shorter and weaker, as revealed by $b_d$ and $b_k$ values (6$^{th}$ May – 13$^{th}$ Jul, 2.1 mg $m^{-3}$).

In the north-western section of the shelf break (R7), the main bloom starts in early-spring ($b_i$ = 27$^{th}$ Aug) and spans until the beginning of summer ($b_e$ = 7th Jan), with a mean peak intensity of

5.37 mg m-3. With a lower probability of occurrence (33 % of the calendar years), the second bloom starts in autumn ($b_i$ = 12th Apr) and it extends for 75 days, with an intensity of 2.5 mg m$^{-3}$. In R8 and R6, corresponding to the location of the shelf-break, the bloom is registered as a single and extended spring-summer bloom ($b_d$ = 173 - 177 days) starting by the end of September, with marked bk differences (5.8 mg m$^{-3}$ and 2.87 mg m$^{-3}$, respectively). The estuarine cold fronts of PCS (R9) also are highly productive in spring and summer ($b_i$ = 15$^{th}$ Oct; $b_e$ = 29$^{th}$ Mar; $b_k$ = 3.01 mg m$^{-3}$).

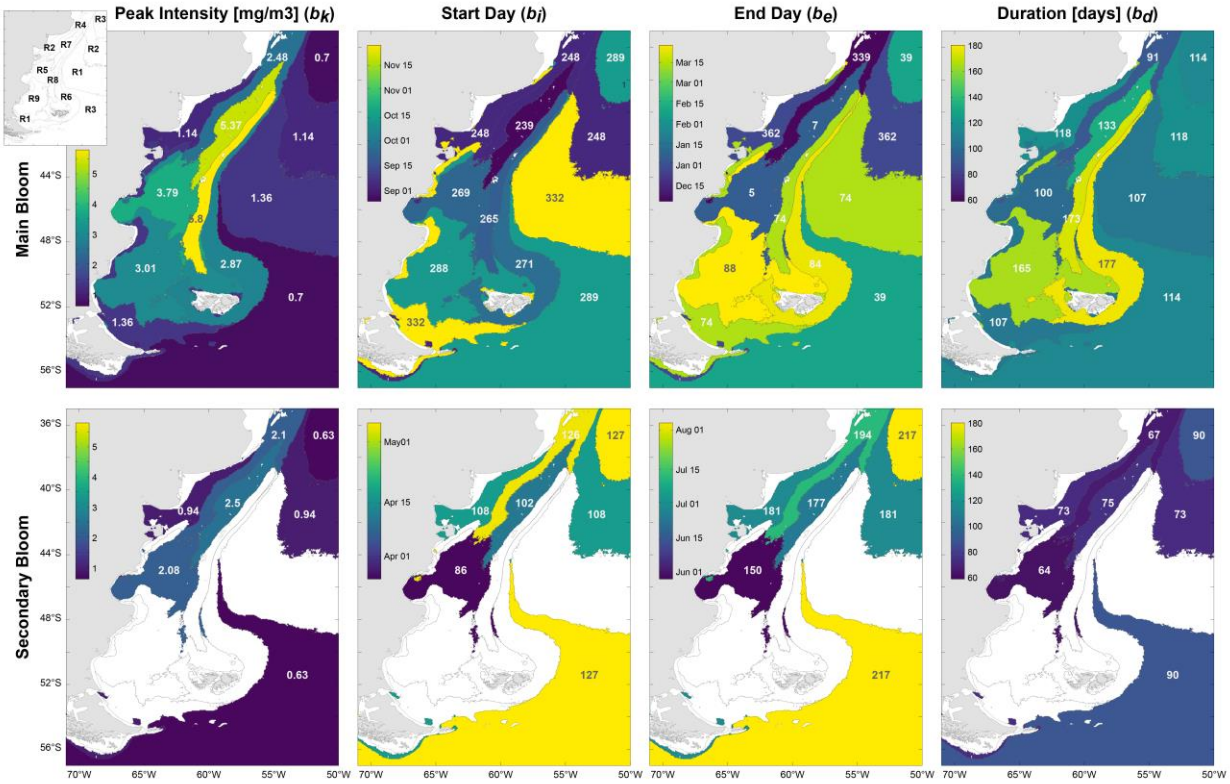


**Figure 3.** Climatology of the main (upper panel) and secondary (lower panel) bloom phenological indices. The $b_i$ and $b_e$ dates are expressed in Julian days. $b_d$ is expressed in days and the $b_k$ in mg Chl-a m$^{-3}$ (Standard deviation and significance values are showed in Table S1 of Supplementary material).

### 3.3 Trends in environmental variables, Chl-a and phytoplankton phenology

A positive significant trend of SST was observed in most of the biogeographical regions, with increases ranging between 0.07 ± 0.02 to 0.26 ± 0.03 °C decade$^{-1}$ (Table 1). Most dramatical changes (> 0.2 °C decade$^{-1}$) occur in R2, whereas trends in the rest of the regions average 0.07 ± 0.04 °C decade-1. A lower negative significant trend was observed on the rest of regions, with higher negative values on R8 and R6 (Malvinas Current; < - 0.15±0.03 °C decade$^{-1}$, Table 1). Even trends in MLD were more geographically variable, a significant negative trend was observed in most of the regions. Largest MLD reduction (< -2.4 ± 0.16 m decade$^{-1}$, Table 1) was restricted to the area covered by R5, R7 and R8. Less productive regions (R1, R2, R3) did not present significant MLD trends. Likewise, Sea Surface Salinity (SSS) showed low or not

significant trends in these regions. Conversely, salinity declines were observed over the highly productive shelf regions (-0.19 ± 0.04 decade$^{-1}$; R4, R5, R7, R9; Table 1).

As shown in Fig.4, with the exception of R1, all regions display a significant positive trend in Chl-a, ranging between 0.03 ± 0.003 at R3 and 0.42 ± 0.04 mg m-3 decade-1 at R7. Regions in the shelf break area, in particular the northern transitional area (R7), showed the highest increases, where the peak intensity of the spring bloom showed a significant rise up to 1.4 ± 0.04 mg m$^{-3}$ decade$^{-1}$ (Fig.5). Also, the Patagonian temperate frontal region (R5) presents a significant Chl-a increase of 0.13 ± 0.001 mg m$^{-3}$ decade$^{-1}$.

| | SST | | MLD | | SSS | |
|---|---|---|---|---|---|---|
| | Trend | p | Trend | p | Trend | p |
| R1 | **0.13±0.02** | **<0.05** | -0.48 | 0.2 | **-0.04±0.004** | **<0.05** |
| R2 | **0.26±0.02** | **<0.05** | -0.43 | 0.28 | -0.02 | 0.37 |
| R3 | **-0.06±0.01** | **<0.05** | -0.35 | 0.71 | -0.02 | 0.06 |
| R4 | 0.09 | 0.07 | **-1.52±0.12** | **<0.05** | **-0.26±0.01** | **<0.05** |
| R5 | **0.08±0.02** | **<0.05** | **-2.49±0.17** | **<0.05** | **-0.19±0.008** | **<0.05** |
| R6 | **-0.15±0.02** | **<0.05** | **1.8±0.46** | **<0.05** | **-0.08±0.008** | **<0.05** |
| R7 | **0.08±0.02** | **<0.05** | **-3.36±0.13** | **<0.05** | **-0.18±0.004** | **<0.05** |
| R8 | **-0.09±0.02** | **<0.05** | **-3.14±0.19** | **<0.05** | **-0.12±0.003** | **<0.05** |
| R9 | -0.07 | 0.05 | **-1.5±0.23** | **<0.05** | **-0.15±0.005** | **<0.05** |

**Table 1.** Trends of SST (°C decade$^{-1}$), MLD (m decade$^{-1}$) and SSS (decade$^{-1}$) for each region defined by SOM analysis (See Fig. 2). Statistically significant trends are highlighted ($p < 0.05$).

Significant trends for the main phenological indices are presented in Fig. 5, considering main and the secondary blooms. The spring-summer bloom starts earlier in R1 ($b_i$ = 28 ± 4 days decade$^{-1}$) and the bloom duration increases ($b_d$ = 41 ± 11 days). Most changes were observed in the secondary blooms of regions within the SAO (R2, R3, R4, R5, R7). The number of autumn blooms in the 24-years period was variable depending on the region considered, but in most regions there was an increasing probability for a second bloom to occur (R2, R3, R4, R5, Table S2 of Supplementary material). Furthermore, three of the five regions presented at least one significant change in the phenology estimates (R2, R3, R5). R5 $b_k$ increase 0.38 ± 0.08 mg m$^{-3}$ decade$^{-1}$, as well as the starting day delayed ($b_i$ = 24 ± 6 days decade$^{-1}$). Also, Region 2 registered a delay of the $b_i$, besides a delay of the bloom termination ($b_e$ = 34 ± 4 days decade$^{-1}$; Fig.5). Finally, in R3 the autumn bloom slightly increases the peak intensity (0.09 ± 0.04 mg m$^{-3}$ decade$^{-1}$), starts earlier and ends later, lengthening the bloom duration in 25 ± 5 days decade$^{-1}$.

## 4 Discussion

### 4.1 Biogeographical regionalization and phenological characterization

An objective regionalization of the SAO has been proposed based on artificial neural networks applied to satellite Chl-a data. We have identified consistent biogeographical regions that correspond to different sub-basins characterized with distinct hydrodynamical, bathymetric or ecological conditions. Two previous supervised and non-supervised regionalization based on Chl-a, SST and SST gradients has been performed for the north-eastern part of the study area

(R1, R2, R3), but with 6-years data and lower spatial resolution (9 km) which resulted in 8 and 12 classes (Saraceno et al., 2005-2006, respectively). Our outcome in that area mostly coincides

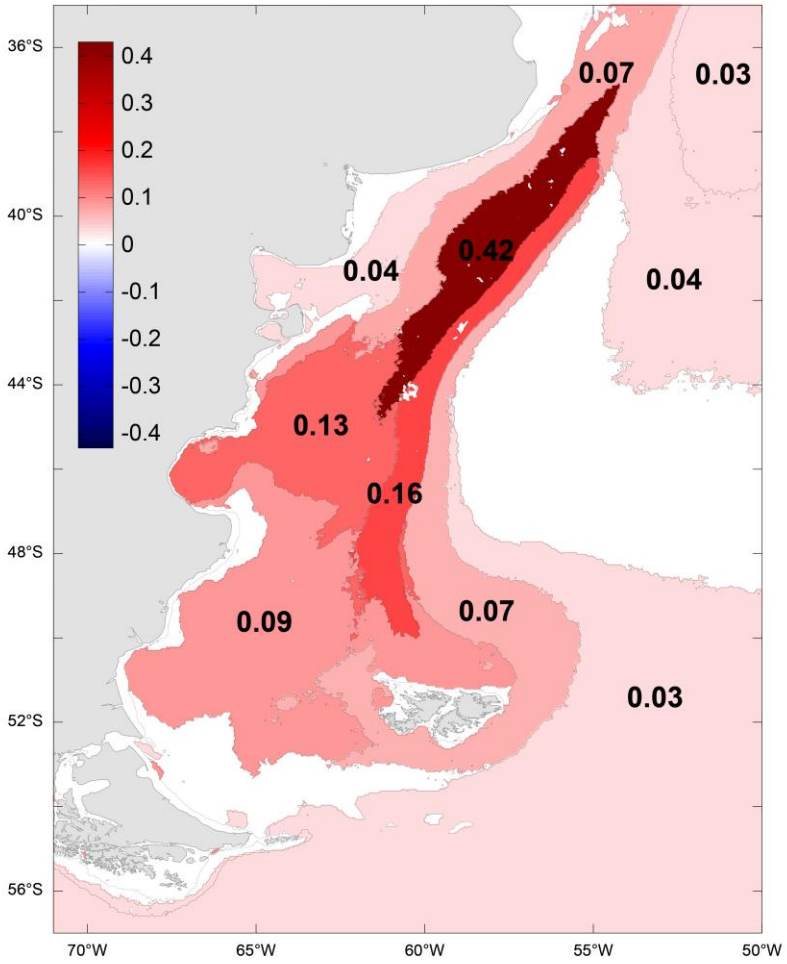


**Figure 4**. 24-years statistically Significant Trends of Chl-a concentration ($p < 0.05$) in the biogeographical regions of the Southern Atlantic Ocean (mg $m^{-3}$ $decade^{-1}$).

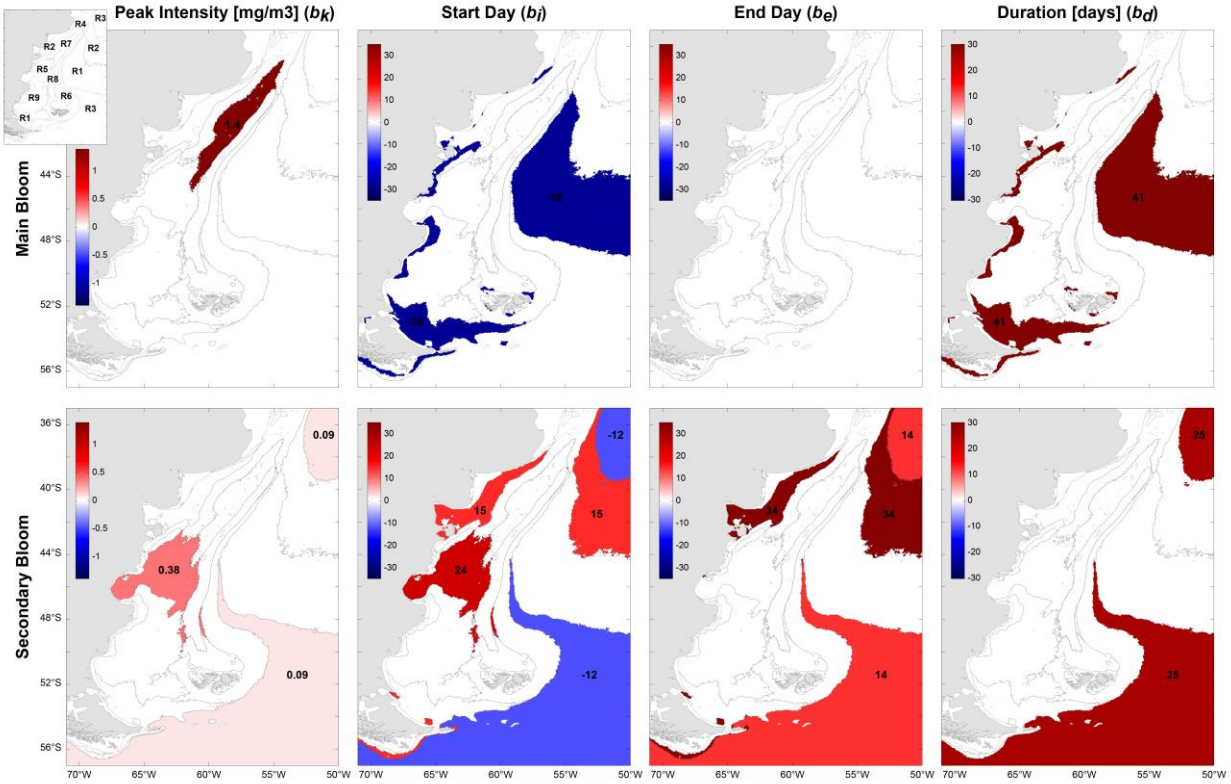


**Figure 5.** Trends of main and secondary phenological indices. $b_k$ is presented in mg $m^{-3}$ $decade^{-1}$ and $b_i$, $b_e$ and $b_d$ in days $decade^{-1}$. Only the regions painted are statistically significant ($p < 0.05$).

with the results presented by Saraceno et al. (2005-2006), where the R3, R2 and R1 are also separated for representing the AO off the Patagonian Shelf.

The biggest depicted region from SOM (R3) includes oligotrophic oceanic waters outside the PCS as well as the Burwood Bank, an undersea bank that forms a barrier to the northward flow of the Antarctic Circumpolar Current and generates conditions that sustain important fisheries (García Alonso et al., 2018; Casarsa et al., 2019). Although it is recognized as a highly productive area (Fig.1), it presents relatively low Chl-a concentrations and phytoplankton biomass. It was suggested that blooms in this area would develop deeper in the water column, due to the presence of fast ocean currents advecting nutrients to the subpolar basin (Matano et al., 2019; Guinder et al., 2020). Two of the largest regions (R1 and R2), which are characterized with relatively low Chl-a concentration, include areas of oceanic and coastal waters with the same Chl-a temporal variability patterns, but with different mechanisms triggering the blooms. R1 includes the coastal Patagonian tidal fronts area, whose location are defined by the boundary between the stratified mid-shelf and the coastal mixed waters. Stratification in the mid-shelf sets during spring-summer is due to the increase in solar radiation, and seasonal fronts develop at the boundary between stratified conditions and tidally mixed coastal waters (Acha et al., 2004). R2, close to the coast, includes the Norpatagonian Gulfs and El Rincón waters (inner shelf). Phenological patterns described for this region agree with previous findings in San Matías Gulf, two phytoplankton biomass patterns were observed: one representing the inner waters, where two blooms were described (autumn-spring), associated with seasonal stratification of the water

column in spring, and bloom decay through summer as a result of nutrient limitation and a maximum in autumn due to a high concentration of nutrients linked to the beginning of the vertical homogenization of the water column; and the mid-shelf waters pattern, where one main bloom with low variability related to the vertical mixing in water column in the coastal areas and light and nitrate availability, developed in late-autumn in the N section and in spring in the S section (Williams et al., 2021). Meanwhile, El Rincón even presents a salinity and a thermal front generated by bathymetry changes and dilution effects, combined with the northern advection of San Matías Gulf waters (Lucas et al., 2005; Rivas and Pisoni, 2010), no clear seasonality of in situ phytoplankton concentration has been reported in this area (Delgado et al., 2015). Both regions, R1 and R2, cover together the retroreflection of BC, which is one of the branches of the SAC, is an eastward conduit of biogenic material on the outer shelf (Signorini et al., 2009). The division in two regions resulted from the SOM is in concordance with Saraceno et al. (2005) where also Chl-a concentration differences was observed. Special attention should be given to the variability and trends of this area, since is a source of productivity for the rest of the South Atlantic Ocean.

The physical mechanisms that trigger the temperate PCS mid-shelf bloom, that covers 9 % of the study area (R5 and R4), are the same, but the blooms result in different bk, bi and be and SOM could successfully separate both. These areas allow for the development of economically important fisheries: The Patagonian temperate fronts (R5) are an important spawning and nursery area of several commercial species (e.g. Argentine red shrimp, Argentine hake, southern king crab, Segura et al. 2021), and R4 is one of the main spring spawning and nursery area for the northern population of E. anochoita (Marrari et al., 2013). The seasonal pattern of these regions agrees with the canonical cycle of temperate seas, where the chlorophyll maxima is associated with the onset of stratification in spring, and a second smaller peak during fall, when the thermocline weakens and deeper nutrient rich waters entrain the surface layer (Carreto et al., 1995; Akselman, 1996; Rivas and Beier, 1990). In R5 both blooms start one month later compared to R4, probably because of later light availability and stratification of the water column for the latitudinal location of the area (southern). The strong peak of R5 is consistent with previous observations in the San Jorge Gulf, where bloom intensity reached ~9 mg $m^{-3}$ (2008) and high values (> 1.5 mg $m^{-3}$) persisted during summer (Fig.2, Segura et al., 2021). The northern Patagonian mid-shelf front (R4) is a ~80 km band of high chlorophyll concentration offshore of the 50 m. During spring-summer the front is developed, by the vertical stratification of waters located ~80 m offshore with a thermocline overlying colder nutrient-rich waters (MC), separating the vertically mixed nutrient-poor coastal waters (R2) (Lucas et al., 2005; Martos and Piccolo, 1988). The end of the bloom in the beginning of summer due to the combined effect of nutrient depletion during the preceding bloom and the development of strong thermal stratification (Carreto et al., 1995).

The shelf-break (SBF) front is a thermohaline permanent front, that broadens and intensifies in spring and summer (Rivas and Pisoni, 2010), delimiting the boundary between the low salinity shelf waters and the colder, saltier and nutrient rich waters of the Malvinas Current (Romero et al., 2006). The persistence of the shelf break bloom is sustained by permanent upwelling of nutrient rich waters (MC) into the euphotic zone caused by the interaction of the MC with bathymetry (Matano and Palma, 2008). Within the Shelf-Break, the bioregionalization allowed for the identification of three different regions, improving our understanding of their triggering mechanisms and their sensibility to environmental forces and changes. The north of the SB (R7)

presents a high inter-annual temporal variability, since it may present one single spring-summer bloom like the rest of SBF (R8) or a spring and autumn bloom, like the MSF (R4), depending on the environmental conditions of a given year. The complex structure of the SBF in this area was analysed by Franco et al. (2008), and a strong Chl-a gradient was described, perpendicular to the front, possibly caused by multiple branches of Malvinas Current. Between the 100 and 1000 m isobath, from 40 °S till the northern-west border of Malvinas Islands, is located R6, a transitional zone between the SBF and the AO. This portion of the SBF is mainly separated by the SOM not because the timing of the bloom (similar to R8), but because the mean values of Chl-a and bk are considerably half lower than the other two regions.

Region R9, encompassing the Patagonian cold estuarine zone, is characterized by a semi-annual cycle. This region is extended from the outer region of the Peninsula Valdez front up to the northern area of Malvinas Islands, overlapping with the south-western portion of the SBF. The water masses located north of the Drake Passage are diluted due to low salinity waters coming from SE Pacific through the Le Marie Strait and the continental run-off of Patagonian main rivers (Lusquiños and Valdéz, 1971; Dai and Trenberth, 2002). The diluted plume, mixed by strong tides and winds (westerlies) is traced till the 100 m isobath and southern San Jorge Gulf (Acha et al., 2004).

### 4.2 Environmental, phytoplankton biomass and phenology trends in the SAO

Western boundary currents are expected to progressively warm as a result of the poleward migration of the subtropical ocean gyres. Indeed, the Brazil Current has been identified as one of the most extensive and intense surface warming hotspots globe wide (Hobday and Pecl, 2014). Our results (see R7 and R2 in Table 1) are consistent with recent studies reporting a warming trend of 0.4° decade$^{-1}$ in the Brazil-Malvinas Confluence and the SBF (e.g. Franco et al., 2020, 2022) as well as in the San Matías and Nuevo Gulfs (Williams and Nocera, 2023). Also, a higher water temperature associated with global warming is predicted over the shelf where the heat exchange between the sea and the atmosphere is strong (Leyba et al., 2019), and this is in agreement with the most pronounced warming trend found in our study.

The depth and properties of the MLD depend on ocean-atmosphere exchanges which are strongly influenced by climate variability (Sallée et al., 2010). Our results indicate consistent shallowing of the MLD (Table 1) and agree with a previous study which address a shoaling trend of the MLD in the Patagonian Shelf (Franco et al., 2023; Williams and Nocera, 2023), with the highest values in the north-western portion of the mid-shelf and the shelf-break (Franco et al., 2022), also in line with the highest trend find in R7 of this study. In the Patagonian shelf the MLD depends mainly on the thermal stratification (Signorini et al., 2006); thus, the increase in SST due to global warming is expected to produce longer periods of shallower MLD (typical of spring and summer), resulting in the negative observed trend.

Sea Surface Salinity (SSS) also presented significant changes in the studied period in most of the regions. All trends are negative, with higher impact in region 4, 5 and 7. The dilution of the northern Patagonian shelf (above ~ -42°) depends mainly on the discharge of major rivers (La Plata, Negro, and Colorado rivers), which are known to present high variability associated to climate variability in general and ENSO events in particular (Acha et al., 2008; Delgado et al., 2015), thus the increase of extreme events associated to climate change (Dai et al., 1997; Hansen

et al., 2006) might be affecting the amount of continental runoff to shelf waters (Pasquini et al., 2010). Possible R2 does not present a negative significant trend, because the salinity on that area also depend on the saline water plume coming from the San Matías Gulf waters which depend on the evaporation over the precipitation balance on the gulf (Lucas et al., 2005). The southern shelf (R1, R9, R5) is diluted mainly for waters coming from the SE Pacific, resulted from glaciers melting and heavy rainfall (> 2000 mm annual), entering in the Argentinean territory through Le Marie strait, and the Santa Cruz River (Luzquiños and Valdéz, 1971; Dai and Trenberth, 2002).

Although the temporal stability of satellite products based on merging data from different sensors, as Globcolour, should be carefully analyzed (Garnesson et al., 2019), in particular for trend computations, our results are consistent with previous positive phytoplankton biomass trends observed in the study area using two sensors (SeaWiFS and MODIS-Aqua: Marrari et al., 2017), or only one sensor (MODIS-Aqua: Franco et al., 2020 and Williams et al., 2023; SeaWiFS: Vantrepotte and Mélin, 2009). The significant trends in Chl-a concentration and phenology indexes presented in this study may be influencing the marine system functioning as they describe changes at the base of the food web, and several factors could be leading these strong trends. In line with our results, previous studies addressed the increasing trend of Chl-a concentration covering then entire Patagonian Shelf or the SBF (Marrari et al., 2017; Franco et al., 2022), but none studies of trends of phenological indices was performed before. Franco et al. (2022) suggested an intensification of the SBF results from a cooling of the MC (SST negative trend in R8, Table 1) and a warming of the adjacent shelf (SST positive trend in R7, Table 1). It combines with the intensification of winds parallel to the front (Risaro et al., 2022) that may enhance the turbulent mixing and increase the upwelling on the onshore side of the front (Franco et al., 2022). All these changes combined would benefit phytoplankton and increase their productivity. On the other hand, we hypothesized that since nutrients are not a limiting factor in the SBF (e.g. Matano and Palma, 2008; Valla and Piola, 2015), a shallower MLD (~ -3.3 m decade-1) might benefit and extended bloom since it enhances the light availability (Franco et al., 2022). Also, there is a succession of phytoplankton groups in the SBF. Typically, a bloom is diatom-dominated in early spring (MLD 40-80 m, nutrient-rich waters), and after nutrient depletion, cocolitophores (Emiliana huxeley) dominate in summer when the MLD reaches its minimum (18 m) (Signorini et al., 2009). Thus, these smaller species could benefit from the negative trend of the MLD. The increasing trend in the Chl-a concentration may be due, not only to a higher phytoplankton biomass, but also to a change in dominance to coccolithophores, as their blooms produce a high concentration of detached coccoliths (plates of calcium carbonate) characterized by a high reflectance (Holligan et al., 1993).

The most sticking changes observed in this study are related to the secondary bloom that appeared in most regions within the PCS. In R2 and R5, a delay in the start of the autumn bloom of 15 and 24 days, respectively was observed. Secondary blooms occur in austral autumn (Apr-May) generally associated with the weakening of the thermocline and the mixing of the water column, supplying nutrient rich bottom waters to the euphotic zone (Akselman, 1996; Rivas and Beier, 1990). The significant warming trend of SST would sustain stratification for a longer period, thus delaying the secondary bloom initialization. Many long-term phytoplankton studies have noted that the timing of the spring bloom is rather constant, occurring approximately the same time each year under highly variable environmental conditions (Eilertsen and Wyatt, 2000), since light is the limitation factor. But, other blooms as may not only be responding physiologically to temperature, they may also respond to temperature indirectly if climate

warming enhances stratified conditions and/or if these conditions appeared earlier (Edwards and Richardson, 2004) or later in the season in the PCS.

## 5 Conclusions

The bioregionalization conducted in the present study allowed the identification, of 9 meaningful areas showing coherent patterns of Chl-a dynamics which are consistent with the oceanographic and biogeochemical characteristics of the Southwestern Atlantic Ocean. The regions permitted to evaluate the areas which have different phenological estimates, mean Chl-a concentration and with different mechanisms triggering the blooms. The regionalization facilitates and improve the analysis of environmental and biological changes in this extensive and highly complex region. The phenology of phytoplankton blooms in these coherent regions have been presented, showing a main seasonal bloom in austral spring (Sep – Dec) in all of them with different timing and intensity, and a secondary peak in austral autumn (Mar– Jun) in some regions, depending on the year.

Significant positive trends in total biomass have been registered in most of regions, with higher Chl-a concentration increase in the shelf-break, especially in the northern area (R7). The remarkable increment in Chl-a concentration of R7 is suggested to be attributed to frontal intensification because of the SST warming, the MLD shoaling and the resulted possible benefit of coccolithophores blooms. In addition, changes in the frequency (more frequent), timing (earlier), and intensity (more intense) of the secondary (autumn) blooms are registered in regions corresponding to the Patagonian temperate front (R5) and the Norpatagonian Gulfs and El Rincón waters (R2). It is suggested that the significant warming trend of SST would sustain stratification for a longer period, thus delaying the secondary bloom initialization This bloom delay could drastically impact on the survival of fish larvae and recruitment as many of the regions are spawning and/or nursey areas, i.e. R2, R4 and R5 (Cushing, 1990). In temperate and high-latitude pelagic ecosystems, may be particularly vulnerable to phenological changes caused by climatic warming, as observed in the SAO. Recruitment success of higher trophic levels is highly dependent on synchronization with seasonally pulsed primary production and the response to regional warming varies among functional groups. Changes in any of these can lead to mismatch in timing between trophic levels (Edwards and Richardson, 2004; Ji et al., 2010).

Although we cannot talk about climate change because our analysis is based on 24 years of data, the observed changes in the main environmental conditions: ocean warming, shoaling of mixed layer depth and less saline seas; are in line with worldwide trends related to climate change estimates (IPCC, 2022). The variations produced by the main environmental drivers associated with the climate change would possibly increase and led to unpredicted results. The depicted bioregionalization and the observed variations in the phytoplankton phenology metrics will be relevant to further investigate the ongoing and future changes, as well as the implications that this might have on higher trophic levels and on commercial fisheries.

## Acknowledgments

The authors would like to thank the Consejo Nacional de Investigaciones Científicas y Técnicas (CONICET) for their financial support (BECA EXTERNA). This research was done in the frame

of I-COOP 2021 project founded by the Consejo Superior de Investigaciones Científicas and the PICT2020-Serie A-02309 founded by the Agencia Nacional de Promoción de la Investigación, el Desarrollo Tecnológico y la Innovación. The present research was carried out within the framework of the activities of the Spanish Government through the "María de Maeztu Centre of Excellence" accreditation to IMEDEA (CSIC-UIB) (CEX2021-001198-M)". I. Hernandez-Carrasco acknowledges financial support from the project TRITOP (grant: UIB2021-PD06) funded by University of the Balearic Islands and by FEDER(EU). V. Combes acknowledges the support of NSF grants OCE-1830856, OCE-2149093, OCE-2149292, NASA award 80NSSC21K0559, and the support from the Spanish Ramón y Cajal Program (RYC2020-029306-I) through grant AEI/UIB - 10.13039/501100011033. J.S Font-Muñoz acknowledges funding by an individual postdoctoral fellowship "Margalida Comas" (PD/018/2020) from Govern de les Illes Balears and Fondo Social Europeo. P. Pratolongo thanks the financial support of Pampa Azul (B8). We all thank the GlobColour and Coopernicus groups for the distribution of satellite merged products and modeled data, respectively.

## Open Research

The Globcolour data can be downloaded from https://hermes.acri.fr/ and the GLORYSv12 data can be downloaded from https://data.marine.copernicus.eu. The SOM v.2.0 MATLAB toolbox can be obtained from http://www.cis.hut.fi/somtoolbox/; the TIMESAT software from https://web.nateko.lu.se/timesat/timesat.asp; the Census X-13 toolbox from https://es.mathworks.com/matlabcentral/fileexchange/49120-x-13-toolbox-for-seasonal-filtering and the Sen's slope estimator from https://es.mathworks.com/matlabcentral/fileexchange/11190-mann-kendall-tau-b-with-sen-s-method-enhanced.

583 **References**

584 Alvain, S., Moulin, C., Dandonneau, Y., & Loisel, H. (2008). Seasonal distribution and
585 succession of dominant phytoplankton groups in the global ocean: A satellite
586 view. *Global Biogeochemical Cycles*, *22*(3). https://doi.org/10.1029/2007GB003154
587 Acha, E. M., Mianzan, H., Guerrero, R., Carreto, J., Giberto, D., Montoya, N., & Carignan, M.
588 (2008). An overview of physical and ecological processes in the Rio de la Plata
589 Estuary. *Continental shelf research*, *28*(13), 1579-1588.
590 https://doi.org/10.1016/j.csr.2007.01.031, 2008
591 Acha, E. M., Mianzan, H. W., Guerrero, R. A., Favero, M., & Bava, J. (2004). Marine fronts at
592 the continental shelves of austral South America: physical and ecological
593 processes. *Journal of Marine systems*, *44*(1-2), 83-105.
594 https://doi.org/10.1016/j.jmarsys.2003.09.005, 2004
595 Anderson, S. I., Barton, A. D., Clayton, S., Dutkiewicz, S., & Rynearson, T. A. (2021). Marine
596 phytoplankton functional types exhibit diverse responses to thermal change. *Nature*
597 *communications*, *12*(1), 6413. https://doi.org/10.1038/s41467-021-26651-8
598 Armstrong, R. A., Gilbes, F., Guerrero, R., Lasta, C., Benavidez, H., & Mianzan, H. (2004).
599 Validation of SeaWiFS-derived chlorophyll for the Rio de la Plata Estuary and adjacent
600 waters. International Journal of Remote Sensing, 25(7-8), 1501-1505.
601 Artana, C., Provost, C., Lellouche, J. M., Rio, M. H., Ferrari, R., & Sennéchael, N. (2019). The
602 Malvinas current at the confluence with the Brazil current: Inferences from 25 years of
603 Mercator ocean reanalysis. *Journal of Geophysical Research: Oceans*, *124*(10), 7178-
604 7200. https://doi.org/10.1029/2019JC015289

Akselman, R. (1996). Estudios ecológicos en el Golfo San Jorge y adyacencias (Atlántico Sudoccidental): Distribución, abundancia y variación estacional del fitoplancton en relación a factores Físico-químicos y la dinámica hidrológica. Doctoral dissertation, Universidad de Buenos Aires. Facultad de Ciencias Exactas y Naturales, https://hdl.handle.net/20.500.12110/tesis_n2857_Akselman.

Basterretxea, G., Font-Muñoz, J. S., Salgado-Hernanz, P. M., Arrieta, J., & Hernández-Carrasco, I. (2018). Patterns of chlorophyll interannual variability in Mediterranean biogeographical regions. *Remote sensing of environment*, *215*, 7-17. https://doi.org/10.1016/j.rse.2018.05.027

Ben Mustapha, Z., Alvain, S., Jamet, C., Loisel, H., & Dessailly, D. (2014). Automatic classification of water-leaving radiance anomalies from global SeaWiFS imagery: application to the detection of phytoplankton groups in open ocean waters. *Remote sensing of environment*, *146*, 97-112. https://doi.org/10.1016/j.rse.2013.08.046

Benzouaï, S., Louanchi, F., & Smara, Y. (2020). Phytoplankton phenology in algerian continental shelf and slope waters using remotely sensed data. *Estuarine, Coastal and Shelf Science*, *247*, 107070. https://doi.org/10.1016/j.ecss.2020.107070

Cai, W., McPhaden, M. J., Grimm, A. M., Rodrigues, R. R., Taschetto, A. S., Garreaud, R. D., ... & Vera, C. (2020). Climate impacts of the El Niño–southern oscillation on South America. *Nature Reviews Earth & Environment*, *1*(4), 215-231. https://doi.org/10.1038/s43017-020-0040-3

Carreto, J., Lutz, V. A., Carignan, M. O., Colleoni, A. D. C., & De Marco, S. G. (1995). Hydrography and chlorophyll a in a transect from the coast to the shelf-break in the

627 Argentinian Sea. *Continental Shelf Research*, *15*(2-3), 315-336.
628 https://doi.org/10.1016/0278-4343(94)E0001-3
629 Casarsa, L., Diez, M. J., Madirolas, A., Cabreira, A. G., & Buratti, C. C. (2019). Morphometric
630 description of schools from two different stocks of the southernmost sprat Sprattus
631 fuegensis. *Fisheries Research*, *212*, 29-34. https://doi.org/10.1016/j.fishres.2018.12.004
632 Cushing, D. H., 1990. Plankton production and year-class strength in fish populations: an update
633 of the match/mismatch hypothesis, in: Advances in marine biology, edited by: J.H.S.
634 Blaxter, A.J. Southward, Vol. 26, Academic Press. https://doi.org/10.1016/S0065-
635 2881(08)60202-3
636 Dai, A., Fung, I. Y., & Del Genio, A. D. (1997). Surface observed global land precipitation
637 variations during 1900–88. *Journal of climate*, *10*(11), 2943-2962. https://doi.org/
638 10.1175/1525-7541
639 Delgado, A. L., Guinder, V. A., Dogliotti, A. I., Zapperi, G., & Pratolongo, P. D. (2019).
640 Validation of MODIS-Aqua bio-optical algorithms for phytoplankton absorption
641 coefficient measurement in optically complex waters of El Rincón
642 (Argentina). *Continental Shelf Research*, *173*, 73-86.
643 https://doi.org/10.1016/j.csr.2018.12.012
644 Delgado, A. L., Loisel, H., Jamet, C., Vantrepotte, V., Perillo, G. M., & Piccolo, M. C. (2015).
645 Seasonal and inter-annual analysis of chlorophyll-a and inherent optical properties from
646 satellite observations in the inner and mid-shelves of the south of Buenos Aires Province
647 (Argentina). *Remote Sensing*, *7*(9), 11821-11847. https://doi.org/10.3390/rs70911821
648 Delgado, A. L., Pratolongo, P. D., Dogliotti, A. I., Arena, M., Celleri, C., Cardona, J. E. G., &
649 Martinez, A. (2021). Evaluation of MODIS-Aqua and OLCI Chlorophyll-a products in

650 contrasting waters of the Southwestern Atlantic Ocean. *Ocean and Coastal Research*, *69*.
651 https://doi.org/10.1590/2675-2824069.20-003ald
652 Dogliotti, A. I., Schloss, I. R., Almandoz, G. O., & Gagliardini, D. A. (2009). Evaluation of
653 SeaWiFS and MODIS chlorophyll-a products in the Argentinean Patagonian continental
654 shelf (38 S–55 S). *International Journal of Remote Sensing*, *30*(1), 251-273.
655 https://doi.org/10.1080/01431160802311133
656 Doney, S. C., Ruckelshaus, M., Emmett Duffy, J., Barry, J. P., Chan, F., English, C. A., ... &
657 Talley, L. D. (2012). Climate change impacts on marine ecosystems. *Annual review of*
658 *marine science*, *4*, 11-37. https://doi.org/10.1146/annurev-marine-041911-111611
659 Drévillon, M., Lellouche, J-M., Réginer, C.,Garric, G., Bricaud, C., Hernandez, O., Bourdallé-
660 Badie, R., 2022. Quality information document for Global Ocean Reanalysis Products.
661 CMEMS-GLO-QUID-001-030.
662 Dutkiewicz, S., Scott, J. R., & Follows, M. J. (2013). Winners and losers: Ecological and
663 biogeochemical changes in a warming ocean. *Global Biogeochemical Cycles*, *27*(2), 463-
664 477. https://doi.org/10.1002/gbc.20042
665 Edwards, M., & Richardson, A. J. (2004). Impact of climate change on marine pelagic
666 phenology and trophic mismatch. *Nature*, *430*(7002), 881-884.
667 https://doi.org/10.1038/nature02808
668 Eilertsen, H. C., & Wyatt, T. (2000). Phytoplankton models and life history strategies. *South*
669 *African Journal of Marine Science*, *22*(1), 323-338.
670 https://doi.org/10.2989/025776100784125717

671 Ferreira, A., Garcia, C. A., Dogliotti, A. I., & Garcia, V. M. (2013). Bio-optical characteristics of
672 the Patagonia Shelf break waters: Implications for ocean color algorithms. *Remote*
673 *sensing of environment*, *136*, 416-432. https://doi.org/10.1016/j.rse.2013.05.022
674 Field, C. B., Behrenfeld, M. J., Randerson, J. T., & Falkowski, P. (1998). Primary production of
675 the biosphere: integrating terrestrial and oceanic components. *science*, *281*(5374), 237-
676 240. https://doi.org/10.1126/science.281.5374.237
677 Franco, B. C., Piola, A. R., Rivas, A. L., Baldoni, A., & Pisoni, J. P. (2008). Multiple thermal
678 fronts near the Patagonian shelf break. *Geophysical Research Letters*, *35*(2).
679 https://doi.org/10.1029/2007GL032066
680 Franco, B. C., Ruiz-Etcheverry, L. A., Marrari, M., Piola, A. R., & Matano, R. P. (2022).
681 Climate change impacts on the Patagonian Shelf break front. *Geophysical Research*
682 *Letters*, *49*(4), e2021GL096513. https://doi.org/10.1029/2021GL096513
683 Franco, B. C., Combes, V., & González Carman, V. (2020). Subsurface ocean warming hotspots
684 and potential impacts on marine species: the southwest South Atlantic Ocean case
685 study. *Frontiers in Marine Science*, *7*, 563394.
686 https://doi.org/10.3389/fmars.2020.563394
687 Friedlingstein, P., Jones, M. W., O'sullivan, M., Andrew, R. M., Hauck, J., Peters, G. P., ... &
688 Zaehle, S. (2019). Global carbon budget 2019. *Earth System Science Data*, *11*(4), 1783-
689 1838. doi.org/10.5194/essd-11-1783-2019
690 García Alonso, V. A., Brown, D., Martín, J., Pájaro, M., & Capitanio, F. L. (2018). Seasonal
691 patterns of Patagonian sprat Sprattus fuegensis early life stages in an open sea Sub-
692 Antarctic Marine Protected Area. Polar Biology, 41, 2167-2179.
693 https://doi.org/10.1007/s00300-018-2352-z

694 Garcia, V. M., Garcia, C. A., Mata, M. M., Pollery, R. C., Piola, A. R., Signorini, S. R., ... &
695 Iglesias-Rodriguez, M. D. (2008). Environmental factors controlling the phytoplankton
696 blooms at the Patagonia shelf-break in spring. *Deep Sea Research Part I: Oceanographic*
697 *Research Papers*, *55*(9), 1150-1166. https://doi.org/10.1016/j.dsr.2008.04.011
698 Garnesson, P., Mangin, A., Fanton d'Andon, O., Demaria, J., & Bretagnon, M. (2019). The
699 CMEMS GlobColour chlorophyll a product based on satellite observation: Multi-sensor
700 merging and flagging strategies. *Ocean Science*, *15*(3), 819-830.
701 Garnesson, P., Mangin, A. and Bretagnon, M.: Quality information document. CMEMS-OC-
702 QUID-009-101to104-116-118, 2.
703 Gilbert, R. O. (1987). *Statistical methods for environmental pollution monitoring*. John Wiley &
704 Sons.
705 Good, S., Fiedler, E., Mao, C., Martin, M. J., Maycock, A., Reid, R., ... & Worsfold, M. (2020).
706 The current configuration of the OSTIA system for operational production of foundation
707 sea surface temperature and ice concentration analyses. *Remote Sensing*, *12*(4), 720.
708 Guinder, V. A., Malits, A., Ferronato, C., Krock, B., Garzón-Cardona, J., & Martínez, A. (2020).
709 Microbial plankton configuration in the epipelagic realm from the Beagle Channel to the
710 Burdwood Bank, a Marine Protected Area in Sub-Antarctic waters. *Plos one*, *15*(5),
711 e0233156. https://doi.org/10.1371/journal.pone.0233156
712 Guinder, V. A., Tillmann, U., Krock, B., Delgado, A. L., Krohn, T., Garzón Cardona, J. E., ... &
713 Lara, R. (2018). Plankton multiproxy analyses in the Northern Patagonian Shelf,
714 Argentina: Community structure, phycotoxins, and characterization of toxic Alexandrium
715 strains. *Frontiers in Marine Science*, *5*, 394. https://doi.org/10.3389/fmars.2018.00394

716 Hansen, J., Sato, M., Ruedy, R., Lo, K., Lea, D. W., & Medina-Elizade, M. (2006). Global
717 temperature change. *Proceedings of the National Academy of Sciences*, *103*(39), 14288-
718 14293. https://doi.org/10.1073/pnas.0606291103
719 Hernández-Carrasco, I., & Orfila, A. (2018). The Role of an Intense Front on the Connectivity of
720 the Western Mediterranean Sea: The Cartagena-Tenes Front. *Journal of Geophysical*
721 *Research: Oceans*, *123*(6), 4398-4422. https://doi.org/10.1029/2017JC013613
722 Hobday, A. J., & Pecl, G. T. (2014). Identification of global marine hotspots: sentinels for
723 change and vanguards for adaptation action. *Reviews in Fish Biology and Fisheries*, *24*,
724 415-425. https://doi.org/10.1007/s11160-013-9326-6
725 Holligan, P. M., Fernández, E., Aiken, J., Balch, W. M., Boyd, P., Burkill, P. H., ... & van der
726 Wal, P. (1993). A biogeochemical study of the coccolithophore, Emiliania huxleyi, in the
727 North Atlantic. *Global biogeochemical cycles*, *7*(4), 879-900.
728 https://doi.org/10.1029/93GB01731
729 Ibanez, F., & Conversi, A. (2002). Prediction of missing values and detection of 'exceptional
730 events' in a chronological planktonic series: a single algorithm. *Ecological*
731 *Modelling*, *154*(1-2), 9-23. https://doi.org/10.1016/S0304-3800(02)00033-9
732 IPCC, 2022: Climate Change 2022: Impacts, Adaptation, and Vulnerability. Contribution of
733 Working Group II to the Sixth Assessment Report of the Intergovernmental Panel on
734 Climate Change. H.-O. Pörtner, D.C. Roberts, M. Tignor, E.S. Poloczanska, K.
735 Mintenbeck, A. Alegría, M. Craig, S. Langsdorf, S. Löschke, V. Möller, A. Okem, B.
736 Rama (eds.). Cambridge University Press. Cambridge University Press, Cambridge, UK
737 and New York, NY, USA, 3056 pp., doi:10.1017/9781009325844

738 Ji, R., Edwards, M., Mackas, D. L., Runge, J. A., & Thomas, A. C. (2010). Marine plankton
739 phenology and life history in a changing climate: current research and future
740 directions. *Journal of plankton research*, *32*(10), 1355-1368.
741 https://doi.org/10.1093/plankt/fbq062
742 Jönsson, P., & Eklundh, L. (2004). TIMESAT—a program for analyzing time-series of satellite
743 sensor data. *Computers & geosciences*, *30*(8), 833-845.
744 https://doi.org/10.1016/j.cageo.2004.05.006
745 Kohonen, T. (1982). Self-organized formation of topologically correct feature maps. *Biological*
746 *cybernetics*, *43*(1), 59-69. https://doi.org/10.1007/BF00337288
747 Kohonen, T. (1990). The self-organizing map. *Proceedings of the IEEE*, *78*(9), 1464-1480.
748 https://doi.org/10.1109/5.58325
749 Lellouche, J. M., Greiner, E., Le Galloudec, O., Garric, G., Regnier, C., Drevillon, M., ... & Le
750 Traon, P. Y. (2018). Recent updates to the Copernicus Marine Service global ocean
751 monitoring and forecasting real-time 1/12∘ high-resolution system. *Ocean Science*, *14*(5),
752 1093-1126. 10.5194/os-14-1093-2018
753 Leyba, I. M., Solman, S. A., & Saraceno, M. (2019). Trends in sea surface temperature and air–
754 sea heat fluxes over the South Atlantic Ocean. Climate Dynamics, 53, 4141-4153.
755 https://doi.org/10.1007/s00382-019-04777-2
756 Liu, Y., Weisberg, R. H., & Mooers, C. N. (2006). Performance evaluation of the self-organizing
757 map for feature extraction. *Journal of Geophysical Research: Oceans*, *111*(C5).
758 https://doi.org/10.1029/2005JC003117
759 Liu, Y., Weisberg, R. H., Vignudelli, S., & Mitchum, G. T. (2016). Patterns of the loop current
760 system and regions of sea surface height variability in the eastern Gulf of Mexico

761 revealed by the self-organizing maps. *Journal of Geophysical Research: Oceans*, *121*(4),
762 2347-2366. https://doi.org/10.1002/2015JC011493
763 Longhurst, A. R. (2010). *Ecological geography of the sea*. Elsevier.
764 Lucas, A. J., Guerrero, R. A., Mianzan, H. W., Acha, E. M., & Lasta, C. A. (2005). Coastal
765 oceanographic regimes of the northern Argentine continental shelf (34–43 S). *Estuarine,*
766 *Coastal and Shelf Science*, *65*(3), 405-420.
767 Lusquiños, A. (1971). *Aportes al conocimiento de las masas de agua del Atlántico*
768 *Sudoccidental* (Vol. 659). Servicio de Hidrografía Naval.
769 Lutz, V. A., Segura, V., Dogliotti, A. I., Gagliardini, D. A., Bianchi, A. A., & Balestrini, C. F.
770 (2010). Primary production in the Argentine Sea during spring estimated by field and
771 satellite models. *Journal of Plankton Research*, *32*(2), 181-195.
772 https://doi.org/10.1093/plankt/fbp117
773 Maritorena, S., d'Andon, O. H. F., Mangin, A., & Siegel, D. A. (2010). Merged satellite ocean
774 color data products using a bio-optical model: Characteristics, benefits and
775 issues. *Remote Sensing of Environment*, *114*(8), 1791-1804.
776 https://doi.org/10.1016/j.rse.2010.04.002
777 Marrari, M., Piola, A. R., & Valla, D. (2017). Variability and 20-year trends in satellite-derived
778 surface chlorophyll concentrations in large marine ecosystems around south and western
779 Central America. *Frontiers in Marine Science*, *4*, 372.
780 https://doi.org/10.3389/fmars.2017.00372
781 Marrari, M., Signorini, S. R., McClain, C. R., Pájaro, M., Martos, P., Viñas, M. D., ... & Buratti,
782 C. (2013). Reproductive success of the A rgentine anchovy, E ngraulis anchoita, in

783 relation to environmental variability at a mid-shelf front (S outhwestern A tlantic O
784 cean). *Fisheries Oceanography*, *22*(3), 247-261. , https://doi.org/10.1111/fog.12019
785 Martos, P., & Piccolo, M. C. (1988). Hydrography of the Argentine continental shelf between 38
786 and 42 S. *Continental Shelf Research*, *8*(9), 1043-1056.
787 Matano, R. P., & Palma, E. D. (2008). On the upwelling of downwelling currents. *Journal of*
788 *Physical Oceanography*, *38*(11), 2482-2500.
789 Matano, R. P., Palma, E. D., & Combes, V. (2019). The Burdwood bank circulation. *Journal of*
790 *Geophysical Research: Oceans*, *124*(10), 6904-6926.
791 https://doi.org/10.1029/2019JC015001
792 Palmer, S. C., Odermatt, D., Hunter, P. D., Brockmann, C., Presing, M., Balzter, H., & Tóth, V.
793 R. (2015). Satellite remote sensing of phytoplankton phenology in Lake Balaton using 10
794 years of MERIS observations. *Remote Sensing of Environment*, *158*, 441-452.
795 https://doi.org/10.1016/j.rse.2014.11.021
796 Pasquini, A. I., & Depetris, P. J. (2010). ENSO-triggered exceptional flooding in the Paraná
797 River: where is the excess water coming from?. *Journal of hydrology*, *383*(3-4), 186-193.
798 https://doi.org/10.1016/j.jhydrol.2009.12.035
799 Racault, M. F., Le Quéré, C., Buitenhuis, E., Sathyendranath, S., & Platt, T. (2012).
800 Phytoplankton phenology in the global ocean. *Ecological Indicators*, *14*(1), 152-163.
801 https://doi.org/10.1016/j.ecolind.2011.07.010
802 Risaro, D. B., Chidichimo, M. P., & Piola, A. R. (2022). Interannual variability and trends of sea
803 surface temperature around Southern South America. *Frontiers in Marine Science*, *9*,
804 213. https://doi.org/10.3389/fmars.2022.829144

Rivas, A. L., & Beier, E. J. (1990). Temperature and salinity fields in the north patagonian gulfs. *Oceanológica acta*, *13*(1), 15-20.

Rivas, A. L., & Pisoni, J. P. (2010). Identification, characteristics and seasonal evolution of surface thermal fronts in the Argentinean Continental Shelf. *Journal of Marine Systems*, *79*(1-2), 134-143. https://doi.org/10.1016/j.jmarsys.2009.07.008

Romero, S. I., Piola, A. R., Charo, M., & Garcia, C. A. E. (2006). Chlorophyll-a variability off Patagonia based on SeaWiFS data. *Journal of Geophysical Research: Oceans*, *111*(C5). https://doi.org/10.1029/2005JC003244

Salgado-Hernanz, P. M., Racault, M. F., Font-Muñoz, J. S., & Basterretxea, G. (2019). Trends in phytoplankton phenology in the Mediterranean Sea based on ocean-colour remote sensing. *Remote Sensing of Environment*, *221*, 50-64. https://doi.org/10.1016/j.rse.2018.10.036

Sathyendranath, S., Brewin, R. J., Brockmann, C., Brotas, V., Calton, B., Chuprin, A., ... & Platt, T. (2019). An ocean-colour time series for use in climate studies: the experience of the ocean-colour climate change initiative (OC-CCI). *Sensors*, *19*(19), 4285. doi:10.3390/s19194285

Saraceno, M., Provost, C., & Lebbah, M. (2006). Biophysical regions identification using an artificial neuronal network: A case study in the South Western Atlantic. *Advances in Space Research*, *37*(4), 793-805. https://doi.org/10.1016/j.asr.2005.11.005

Saraceno, M., Provost, C., & Piola, A. R. (2005). On the relationship between satellite-retrieved surface temperature fronts and chlorophyll a in the western South Atlantic. *Journal of Geophysical Research: Oceans*, *110*(C11). https://doi.org/10.1029/2004JC002736

827 Sallée, J. B., Speer, K. G., & Rintoul, S. R. (2010). Zonally asymmetric response of the Southern
828 Ocean mixed-layer depth to the Southern Annular Mode. *Nature Geoscience*, *3*(4), 273-
829 279. https://doi.org/10.1038/ngeo812
830 Segura, V., Silva, R. I., Clara, M. L., Martos, P., Cozzolino, E., & Lutz, V. A. (2021). Primary
831 production and plankton assemblages in the fisheries ground around San Jorge Gulf
832 (Patagonia) during spring and summer. *Plankton and Benthos Research*, *16*(1), 24-39.
833 https://doi.org/10.3800/pbr.16.24
834 Shi, K., Zhang, Y., Zhang, Y., Li, N., Qin, B., Zhu, G., & Zhou, Y. (2019). Phenology of
835 phytoplankton blooms in a trophic lake observed from long-term MODIS
836 data. *Environmental science & technology*, *53*(5), 2324-2331.
837 https://doi.org/10.1021/acs.est.8b06887
838 Shiskin, J. (1978). Seasonal adjustment of sensitive indicators. In *Seasonal Analysis of Economic*
839 *Time Series* (pp. 97-104). NBER.
840 Sigman, D. M., Hain, M. P., & Haug, G. H. (2010). The polar ocean and glacial cycles in
841 atmospheric CO2 concentration. *Nature*, *466*(7302), 47-55.
842 https://doi.org/10.1038/nature09149
843 Signorini, S. R., Garcia, V. M., Piola, A. R., Evangelista, H., McClain, C. R., Garcia, C. A., &
844 Mata, M. M. (2009). *Further studies on the physical and biogeochemical causes for large*
845 *interannual changes in the Patagonian Shelf spring-summer phytoplankton bloom*
846 *biomass* (No. 200900836).
847 Signorini, S. R., Garcia, V. M., Piola, A. R., Garcia, C. A., Mata, M. M., & McClain, C. R.
848 (2006). Seasonal and interannual variability of calcite in the vicinity of the Patagonian
849 shelf break (38 S–52 S). *Geophysical research letters*, *33*(16).

Spalding, M. D., Fox, H. E., Allen, G. R., Davidson, N., Ferdaña, Z. A., Finlayson, M. A. X., ... & Robertson, J. (2007). Marine ecoregions of the world: a bioregionalization of coastal and shelf areas. *BioScience*, *57*(7), 573-583. https://doi.org/10.1641/B570707

Valla, D., & Piola, A. R. (2015). Evidence of upwelling events at the northern P atagonian shelf break. *Journal of Geophysical Research: Oceans*, *120*(11), 7635-7656. https://doi.org/10.1002/2015JC011002

Vantrepotte, V., & Mélin, F. (2009). Temporal variability of 10-year global SeaWiFS time-series of phytoplankton chlorophyll a concentration. *ICES Journal of Marine Science*, *66*(7), 1547-1556. https://doi.org/10.1093/icesjms/fsp107

Vantrepotte, V., & Mélin, F. (2011). Inter-annual variations in the SeaWiFS global chlorophyll a concentration (1997–2007). *Deep Sea Research Part I: Oceanographic Research Papers*, *58*(4), 429-441. https://doi.org/10.1016/j.dsr.2011.02.003

Vesanto, J., & Alhoniemi, E. (2000). Clustering of the self-organizing map. *IEEE Transactions on neural networks*, *11*(3), 586-600. https://doi.org/10.1109/72.846731

Vesanto, J., Himberg, J., Alhoniemi, E., Parhankangas, J., Team, S. O. M. T., & Oy, L. (2000). *SOM toolbox for Matlab 5* (Vol. 57, No. 2). Technical report.

Williams, G. N., Pisoni, J. P., Solís, M. E., Romero, M. A., Ocampo-Reinaldo, M., Svendsen, G. M., ... & González, R. A. C. (2021). Variability of phytoplankton biomass and environmental drivers in a semi-enclosed coastal ecosystem (San Matías Gulf, Patagonian Continental Shelf, Argentina) using ocean color remote sensing (MODIS) and oceanographic field data: Implications for fishery resources. *Journal of Marine Systems*, *224*, 103615. https://doi.org/10.1016/j.jmarsys.2021.103615

Williams, G. N., Dogliotti, A. I., Zaidman, P., Solis, M., Narvarte, M. A., Gonzalez, R. C., ... & Gagliardini, D. A. (2013). Assessment of remotely-sensed sea-surface temperature and chlorophyll-a concentration in San Matías Gulf (Patagonia, Argentina). *Continental Shelf Research*, *52*, 159-171. https://doi.org/10.1016/j.csr.2012.08.014

Williams, G. N., & Nocera, A. C. (2023). Bio-optical trends of waters around Valdés Biosphere Reserve: An assessment of the temporal variability based on 20 years of ocean color satellite data. *Marine Environmental Research*, 105923. https://doi.org/10.1016/j.marenvres.2023.105923

Yala, K., Niang, N. D., Brajard, J., Mejia, C., Ouattara, M., El Hourany, R., ... & Thiria, S. (2020). Estimation of phytoplankton pigments from ocean-color satellite observations in the Senegalo–Mauritanian region by using an advanced neural classifier. *Ocean Science*, *16*(2), 513-533. https://doi.org/10.5194/os-16-513-2020

Yu, S., Bai, Y., He, X., Li, T., & Gong, F. (2023). A new merged dataset of global ocean chlorophyll-a concentration for better trend detection. *Frontiers in Marine Science*, *10*, 48. https://doi.org/10.3389/fmars.2023.1051619

Zhai, L., Platt, T., Tang, C., Sathyendranath, S., & Walne, A. (2013). The response of phytoplankton to climate variability associated with the North Atlantic Oscillation. *Deep Sea Research Part II: Topical Studies in Oceanography*, *93*, 159-168. https://doi.org/10.1016/j.dsr2.2013.04.009

Zoljoodi, M., Moradi, M., & Moradi, N. (2022). Seasonal and interannual cycles of total phytoplankton phenology metrics in the Persian Gulf using ocean color remote sensing. *Continental Shelf Research*, *237*, 104685. https://doi.org/10.1016/j.csr.2022.104685